Conversion of transverse momentum correlation of photon pairs into polarization entanglement by using wavefront-splitting interference

Csaba Tamás Holló,[1,*] Tamás Sarkadi,[1] Máté Galambos,[2] Attila Barócsi,[1] Pál Koppa,[1] Veronika Hanyecz,[3] and Gábor Erdei[1]

[1]*Department of Atomic Physics, Institute of Physics, Budapest University of Technology and Economics, Műegyetem rkp. 3., H-1111 Budapest, Hungary*

[2]*Department of Networked Systems and Services, Budapest University of Technology and Economics, Műegyetem rkp. 3., H-1111 Budapest, Hungary*

[3]*ELI-ALPS, ELI-HU Non-Profit Limited, Wolfgang Sandner u. 3, H-6728 Szeged, Hungary*

(Received 23 May 2022; accepted 25 November 2022; published 15 December 2022)

The transverse momentum correlation of photon pairs generated by noncollinear spontaneous parametric down-conversion with type-I phase matching is transformed into polarization entanglement. A robust wavefront-splitting interferometer scheme is used, due to which the phase of the entangled state does not require active stabilization. Frequency-degenerate signal and idler photons are separated and coupled into single-mode optical fibers. The concept is demonstrated in a compact and modular setup. A straightforward alignment process for producing any of the Bell states is presented. The entangled source has an output photon flux of 8.33 ± 1.27 kcps/mW normalized to pump power (150 mW), and $17 \pm 3\%$ heralding ratio. The measured state fidelity with respect to the negative anticorrelated Bell state is 0.951 ± 0.004.

DOI: 10.1103/PhysRevA.106.063710

I. INTRODUCTION

Sources of entangled photon pairs are of key importance in the demonstration as well as the practical utilization of many quantum-optical phenomena. Nowadays, their primary application is found in quantum cryptography, since many protocols of secure key distribution rely on entanglement [1–3], which is a typical manifestation of temporal quantum correlation. Other prospective areas include optical quantum computers [4,5] together with a link and distribution of entanglement between them [6,7]. Most of these require conveniently usable sources with similar specifications, and photon pairs coupled into single-mode optical fibers.

A broad variety of entangled photon pair generation methods exist in the literature, providing temporal correlation between any property of the photons: position, momentum, energy, phase, or polarization. From these presently the latter seems to be the most useful in quantum cryptography, the application field of our main concern. A common technique to produce correlated photon pairs utilizes the nonlinear process of spontaneous parametric down-conversion (SPDC). With its help polarization entanglement can be achieved, e.g., by making use of momentum correlation in a noncollinear type-II phase-matching configuration by collecting photons at the intersection points of the two resultant orthogonally polarized light cones [8]. This method is the oldest one, offering a rather low conversion efficiency. Another solution is to produce SPDC in two subsequent independent crystals [9–11], yielding higher conversion and collection efficiency, although requiring twice the amount of nonlinear material and a precise alignment of the two crystals relative to each other. It is also common to pump the same crystal with multiple beams coherently [12–15], where the greatest difficulty occurs at aligning the beams and maintaining their relative phase. In another case the correlation of the birth position of the pairs is transformed to polarization entanglement [16]. Though the applied wavefront-splitting interferometer provides a robust setup, the implemented collinear arrangement prohibits the separation of frequency-degenerate pairs. Since this latter characteristic is desired in many applications, mainly in linear optical quantum computation and distributed quantum networks, both requiring sources of identical photons [17–19], we decided to develop a setup that not only retains the stability of wavefront-splitting interferometry but also features frequency degeneration.

This paper presents how to transform momentum correlation into polarization entanglement in a noncollinear type-I phase-matching configuration by using a wavefront-splitting interferometer setup. Details of the concept and a specific demonstrative implementation of our method are given, resulting in a single-mode fiber-coupled photon pair source. The method inherently does not separate the optical paths of different polarization states, and therefore does not require active, interferometric stabilization. Along with the description of the equipment, a straightforward alignment process for generating any of the Bell states on the detection side is presented. Photon and coincidence rates, density matrix, and state fidelity of the source are measured.

II. CONCEPT AND EXPERIMENTAL SETUP

Besides conservation of energy, photons generated by the type-I SPDC process must obey momentum conservation, i.e.,

*hollo.csaba@ttk.bme.hu

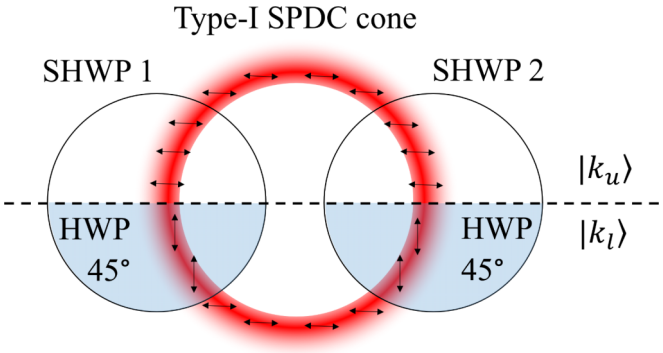

FIG. 1. Segmented half-wave plates (SHWPs) in the far field of the SPDC light source, both having two sections. The lower one contains a quartz half-wave plate (HWP) oriented at 45° with respect to the horizontal polarization of down-converted photons, and the upper part is isotropic fused silica of the same thickness. In consequence, the polarization of light propagating through the upper segment in the $|k_u\rangle$ momentum state remains unchanged, while in the lower segment (i.e., $|k_l\rangle$ state) it is transformed to the vertical direction. Arrows indicate the direction of polarization along the SPDC cone. Details of coupling down-converted light into optical fibers can be found in Ref. [20].

phase matching too. In a noncollinear setup the wave function of the resultant photon pairs propagates in a cone centered to the axis of the pump, with each photon having the same polarization. One can separate the members of these pairs in terms of transverse momentum by collecting them with two apertures placed in the far-field of the nonlinear crystal at axially symmetric positions along the cone. Here, "transverse" refers to a direction orthogonal to the pump axis. If we consider the transverse momentum of SPDC photons sorted into two categories $|k_u\rangle$ and $|k_l\rangle$ propagating in the upper and lower part of the light cone, respectively (i.e., above or below the dashed meridional line in Fig. 1), then the momentum-correlated wave function can be written in the form of Eq. (1), where $\otimes$ denotes the Kronecker product of state vectors, and $|h\rangle$ describes the horizontal polarization of the SPDC cone:

$$|\psi\rangle = \frac{|k_u\rangle|k_l\rangle \otimes |h\rangle|h\rangle + |k_l\rangle|k_u\rangle \otimes |h\rangle|h\rangle}{\sqrt{2}}. \tag{1}$$

In our concept, illustrated in Fig. 1, we place a segmented half-wave plate (SHWP) in front of both apertures, each having two parts of equal area. The lower half is a zero-order quartz half-wave plate (HWP) with its optical axis oriented at 45° with respect to the $|h\rangle$ polarization of the SPDC cone. The upper section is filled with fused silica of equivalent optical thickness as that of the quartz, to compensate for the phase shift accumulated by the beam propagating through the lower section. The operation of these rotated HWPs can be best described in the basis of the diagonal $|d\rangle$ and antidiagonal $|a\rangle$ state vectors. Retarders introduce a phase shift of α between these states, which is π in case of ideal half-wave plates,

$$|h\rangle \to |d\rangle + e^{i\alpha}|a\rangle = |d\rangle - |a\rangle = |v\rangle, \tag{2}$$

meaning that a half-wave retarder transforms $|h\rangle$ into $|v\rangle$. Also, from Eq. (2) we can understand that orientation and retardation accuracy is crucial, so any deviations from optimum settings deteriorate the state fidelity. The $|\psi'\rangle$ wave function after the SHWPs is formulated as Eq. (3).

$$|\psi'\rangle = \frac{|k_u\rangle|k_l\rangle \otimes |h\rangle|v\rangle + |k_l\rangle|k_u\rangle \otimes |v\rangle|h\rangle}{\sqrt{2}}. \tag{3}$$

After both apertures, the photons are focused and coupled into single-mode optical fibers by appropriate imaging systems (typically lenses). The mode overlap between the focused $|k_u\rangle_1 \otimes |h\rangle$ SHWP1 upper segment, and the $|H\rangle$ horizontally polarized propagating mode in the fiber can be described as a complex c_{h1} coupling amplitude:

$$c_{\mathrm{h1}} = \langle H|(|k_u\rangle_1 \otimes |h\rangle). \tag{4}$$

The same stands for the vertically polarized lower segment of SHWP1 and for the two segments of SHWP2 with $c_{\mathrm{v1}}, c_{\mathrm{h2}}, c_{\mathrm{v2}}$ amplitudes, respectively, the absolute squares of which determine the fiber-coupling efficiency of each segment. Using the above, one can formulate the $|\Psi\rangle$ fiber-coupled expression of the wave function as

$$|\Psi\rangle = \frac{c_{\mathrm{h1}}|H\rangle c_{\mathrm{v2}}|V\rangle + c_{\mathrm{v1}}|V\rangle c_{\mathrm{h2}}|H\rangle}{\sqrt{|c_{\mathrm{h1}}c_{\mathrm{v2}}|^2 + |c_{\mathrm{v1}}c_{\mathrm{h2}}|^2}}, \tag{5}$$

where $|V\rangle$ denotes the vertically polarized fiber mode. Equation (5) can be interpreted as the focusing lenses coherently coupling the $|h\rangle|v\rangle$ and $|v\rangle|h\rangle$ states into the fibers with $c_{\mathrm{h1}}c_{\mathrm{v2}}$ and $c_{\mathrm{v1}}c_{\mathrm{h2}}$ amplitudes, respectively. For simplification we introduce

$$ce^{i\Delta\varphi} \equiv \frac{c_{\mathrm{v1}}c_{\mathrm{h2}}}{c_{\mathrm{h1}}c_{\mathrm{v2}}} \quad \text{and} \quad \phi \equiv \arg(c_{\mathrm{h1}}c_{\mathrm{v2}}), \tag{6}$$

with which the entangled state can be formulated as

$$|\Psi\rangle = e^{i\phi}\frac{|H\rangle|V\rangle + ce^{i\Delta\varphi}|V\rangle|H\rangle}{\sqrt{1+c^2}}. \tag{7}$$

It must be noted here that ϕ has no effect on the operation of the photon source at all, thus we will not deal with it in further discussions.

The schematic illustration of our fiber-coupling system is depicted in Fig. 2. A beta barium borate (BBO) crystal is pumped at 405 nm by 150 mW power to produce frequency-degenerate photon pairs at 810 nm center wavelength. The pump is blocked by the filter F and obscurations at the A apertures. By choosing F to be a long-pass filter, we obtain a photon source of wide spectral bandwidth, while applying a narrow-band filter results in quasimonochromatic down-converted photons. The pairs are separated by the M mirrors, and directed towards the fiber-coupling optics. Design considerations and details of the optical setup are given in Refs. [20,21].

The only distinct difference from our previous implementation is that here we use standard single-mode fibers instead of polarization-maintaining ones in order to minimize the phase shift between polarization modes. Not being available as commercial products, the segmented half-wave plates were fabricated in the optical workshop of the Department of Atomic Physics, and serve primarily demonstrative purposes. We used 3-mm-thick, 20 × 20 mm rectangular glass slabs as

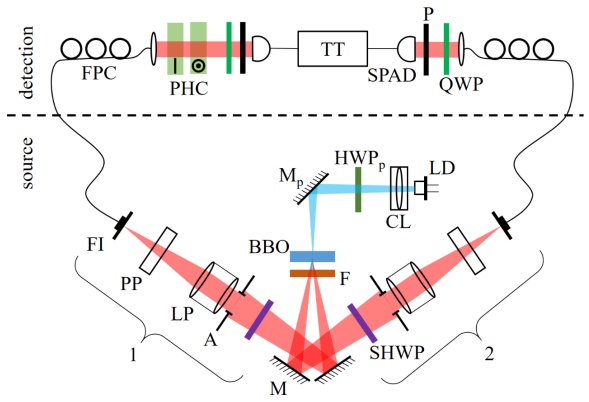

FIG. 2. Schematics of the experimental setup. Blue and red beams indicate pump and down-converted light, respectively. LD: laser diode; CL: focusing assembly; M_p: pump fold mirror; HWP_p: half-wave plate for the pump; F: spectral filter; M: dielectric "hot" mirror (reflects wavelengths between 750 and 1100 nm); SHWP: segmented half-wave plate; A: aperture; LP: relaying lens pair; PP: plane-parallel plate; FI: fiber input (for details of the source, see Ref. [20]); FPC: fiber polarization controller; PHC: anisotropic phase compensator with optical axis indicated; SPAD: single-photon avalanche detector; TT: time tagger; QWP: quarter-wave plate; P: linear polarizer.

substrates, on each of which a properly oriented single-crystal quartz and a fused silica plate were cemented in adjacent position. This construction results in a sharp edge between the two parts, minimizing photon loss. Both plates were of 10×20 mm size and ground/polished together, resulting in identical thicknesses and a diffraction-limited transmitted wavefront. In order to have true zero-order phase retarders the target thickness was 45.5 μm, which we met by ±2 μm accuracy according to our measurements. Multiple SHWPs were manufactured and characterized with 809-nm laser light and linear polarizers to determine the wave-plate thickness and orientation. Based on these evaluations, the best two were selected for the source. Consequences of fabrication errors will be discussed in the Results section.

Strictly speaking, Eq. (7) is valid only at the beginning of the fiber. Losses degrade the magnitude of c if they are asymmetrically present in the fibers. Relying on the manufacturing tolerances we consider these as negligible. Stress-induced anisotropy and axial twisting of the fibers act together as an arbitrary unitary polarization transform, which varies both $\Delta\varphi$ and the basis of polarization correlation. These can be utilized to set the desired Bell state at the detection side by using a well-known technique that implements phase retarders as fiber loops. In order to control the polarization state at the fiber outputs, we created three appropriate loops on both fibers to form two stacks of quarter-half-quarter-wave retarders, depicted as FPC in Fig. 2. So that we can adjust $\Delta\varphi$ in Eq. (7) separately from other polarization changes in the fibers, we constructed a simple phase compensator, indicated by PHC in Fig. 2. This consists of two antireflection-coated uniaxial birefringent crystals made of lithium niobate ($LiNbO_3$) with optical axes oriented orthogonally in the horizontal-vertical basis. The two subsequently placed crystals have equal thickness in order to cancel the combined phase shift when both are perpendicular to the incident beam. Tilting one of them around its optical axis changes the effective crystal length, therefore the optical path difference between $|H\rangle$ and $|V\rangle$, which affects $\Delta\varphi$. An advantage of our wavefront-splitting interferometer setup is that $\Delta\varphi$ is insensitive to any path-length differences between the optical arms, such as mechanical vibrations or thermal dilation. Only time-dependent perturbations in the fibers must be compensated, otherwise there is no need for active stabilization in the source.

A measuring basis for the desired Bell state is set at the detection side. Since measurements in different Bell states can be accomplished by using simple polarization transformations, here we present the adjustment of only one example, viz., the $|\Psi^-\rangle$ negative anticorrelated Bell state, where $\Delta\varphi = \pi$ and $c = 1.0$ in Eq. (7). Owing to wavefront-splitting interferometry used in our source, this process is relatively easy and takes only two steps.

First step: We start by preparing the polarization analyzers (consisting of a QWP quarter-wave plate and a P linear polarizer) in front of the detectors to measure exclusively the $|V\rangle$ state. We cover the lower part of both SHWPs and tune the FPC fiber polarization controllers to minimize detector counts on both sides. In this way the whole system, including the fibers, transforms the polarization of light incident on the upper part of the SHWP-s to the $|H\rangle$ state. The lower parts of the SHWP-s always produce an orthogonal polarization with respect to the upper (as long as the transformation made by the fibers can be considered unitarian), in this case $|V\rangle$. (Setting the linear polarization on one detector *orthogonal* relative to the other corresponds to the correlated state.) Although the suitable polarization basis is now set, we still have to adjust $\Delta\varphi$—this is done in the *second step*. To begin with, the baffles that cover the lower half of the SHWPs are removed. Then both analyzers are realigned to measure the $|D\rangle = |H\rangle + |V\rangle$ state. In this position we adjust the phase $\Delta\varphi$ by using the phase compensator as described above, until minimal coincidence counts are detected to reach $\Delta\varphi = \pi$. (The maximum coincidence in the $|D\rangle$ state corresponds to $\Delta\varphi = 0$.)

Our source is modular in terms of bandwidth of the generated photon pairs and polarization entanglement. One can easily reconfigure the setup by changing the F filter or inserting/removing the SHWPs. Only a minor realignment is necessary concerning the focus position of the LP lenses and tilting of the PP plane-parallel plates in front of the fiber inputs (see Ref. [20]).

III. RESULTS

We have measured some of the most important properties of our demonstrator device operated in different modes. All the values listed in Table I were determined at the fiber outputs and include a correction for detector efficiency, as if they were measured with detectors of 100% efficiency (the calculation is detailed in Ref. [20]).

The results clearly show that spectral filtering is beneficial in terms of the $\mathbb{P}_h$ heralding ratio, the explanation of which originates in losses. Every absorption, scattering, reflection, or the fiber-coupling efficiency decrease the value of $\mathbb{P}_h$. From these it is by far the latter that reduces heralding ratio the most in our setup. Since there is always some residual chromatic

TABLE I. Optical properties of the photon source in different operational modes. Photon flux Φ_s, coincidence flux Φ_s^c, and heralding ratio $\mathbb{P}_h$ are measured at the single-mode fiber outputs, normalized to pump power (150 mW). All values are corrected for detector efficiency, and the errors indicated correspond to 1 standard deviation.

Filtering	Polarization entanglement	Φ_s (kcps/mW)	Φ_s^c (kcps/mW)	$\mathbb{P}_h$ (%)	Bandwidth (nm)
Long pass from 600 nm	No	636 ± 95	130 ± 39	20 ± 3	202
Bandpass at 810 nm	No	17.3 ± 2.6	6.8 ± 1.1	39 ± 6	10
Bandpass at 810 nm	Yes	8.33 ± 1.27	1.47 ± 0.23	17 ± 3	10

aberration even in achromatic systems, the wave function of narrow-band photons can be better focused on the fiber inputs, resulting in a higher coupling efficiency, thus larger $\mathbb{P}_h$. The presence of the SHWPs decreases heralding ratio in a similar way. The segmented half-wave plates bisect the apertures, forcing the upper and lower halves to couple to orthogonal polarization modes independently of each other. This causes a drop in coupling efficiency, since the focus spot size of the LP lenses doubles in the vertical direction due to diffraction by the smaller apertures. By using ZEMAX OPTICSTUDIO [22] we calculated a fiber-coupling efficiency of 50.9% for a light cone section covering the whole aperture A [20], whereas the same calculation yielded 23.4% for a half aperture. Since the heralding ratio and the Φ_s photon flux have a linear, and the Φ_s^c coincidence flux has a quadratic dependence on the fiber-coupling efficiency, from these values we expected Φ_s and $\mathbb{P}_h$ to drop to 46.0%, while Φ_s^c to 21.1% of its original value when inserting the SHWPs. These changes agree with those found in Table I within error margin, hence the ZEMAX simulation can be accepted as a plausible explanation for our measurement experiences.

We also measured the ρ density matrix of the system. For this we adjusted the setup to produce the previously mentioned $|\Psi^-\rangle$ Bell state and conducted a full state tomography [23]. Results are depicted in Fig. 3. State fidelity towards the $|\Psi^-\rangle$ state, with a corresponding theoretical density matrix of $\sigma = |\Psi^-\rangle\langle\Psi^-|$, was calculated according to definition as Eq. (8),

$$F(\rho,\sigma) = \left(\mathrm{tr}\sqrt{\sqrt{\rho}\sigma\sqrt{\rho}}\right)^2 = 0.945, \tag{8}$$

and also from visibility (V) measurements [24]. In the horizontal-vertical basis we got $V_{H/V} = 0.921 \pm 0.008$, in the diagonal-antidiagonal basis $V_{D/A} = 0.971 \pm 0.006$, while in the left-right circular basis $V_{R/L} = 0.913 \pm 0.013$. Fidelity ($F$), as defined by Eq. (9), was found to be $F = 0.951 \pm 0.004$:

$$F(\rho,\sigma) = \frac{1 + V_{H/V} + V_{D/A} + V_{R/L}}{4}. \tag{9}$$

Neither the density matrix nor the fidelity shows a perfect match with the desired $|\Psi^-\rangle$ state. According to the operation principle of SHWPs [described by Eq. (2)], we identified their manufacturing errors as the major cause of deviation. Inaccuracies during the fabrication of the crystalline quartz lower half of the segmented half-wave plates results in thickness and orientation variations from the nominal, which deteriorates the linear polarization of SPDC photons. In order to find out the source and magnitude of the polarization errors, we performed further, supplementary measurements.

The polarization states were analyzed at the fiber outputs with a rotatable linear polarizer of 1:1000 extinction ratio. During the measurements only the lower or the upper half of the SHWPs were allowed to transmit light, while the other half was covered. In this way, we determined the power ratio between the major and minor axes (i.e., the extinction ratio) and the orientation angle of the polarization ellipse with respect to the horizontal-vertical basis in each SHWP segment. The results are summarized in Table II; values corresponding to the upper fused silica plates serve as a reference. Data obtained for the lower apertures, where the crystalline quartz HWPs are located, reveal significant misorientation in the case of SHWP1, and a rather low extinction ratio. This implies that the thickness of SHWP1 was not fabricated as planned. In consequence, when we make coincidence measurements, the highly linear polarization at the SHWP2 upper section is correlated with a not perfectly orthogonal and slightly elliptic polarization at SHWP1 lower section. This results in product states also appearing in the experimentally generated mixture, which degrades state fidelity and the density matrix. Replacing our demonstrative SHWPs with more accurate ones would obviously overcome this problem.

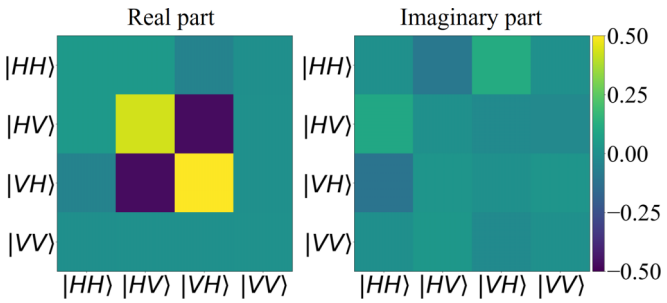

FIG. 3. Measured ρ density matrix of the generated polarization entangled state.

TABLE II. Experimentally obtained polarization states after each segment of the SHWPs. Power ratio between the major and minor axes (extinction ratio), and orientation angle of the polarization ellipse with respect to the horizontal-vertical basis were measured. SHWP1(2)$_{u(l)}$ denote the upper (lower) part of the first (second) segmented wave plate, respectively.

Segment	Extinction ratio	Orientation (deg)
SHWP1$_u$	401 ± 71	0 ± 1
SHWP2$_u$	410 ± 81	0 ± 1
SHWP1$_l$	29.1 ± 0.71	12.5 ± 1
SHWP2$_l$	511 ± 65	3 ± 1

IV. CONCLUSION

We presented a method for the realization of polarization entanglement in a wavefront-splitting interferometric setup consisting of the minimum number of optical elements and without a need for active phase stabilization. The demonstrator device is compact, modular, and offers convenient applicability by providing photon pairs coupled directly into single-mode fibers. The measurable entangled state purity is only a matter of fabrication accuracy of the used segmented half-wave plates. Its current characteristics make the equipment suitable for, e.g., free-space telecommunication purposes [25] due to the 810 nm wavelength of generated photons, or clock synchronization [26], just to mention a few possible applications. Our approach can also be adopted to any other noncollinear SPDC geometries, applying even different nonlinear crystals. For instance, the photon flux can be easily boosted by replacing the BBO with a periodically poled potassium titanyl phosphate crystal that has greater down-conversion efficiency. The currently achieved heralding ratio might be increased by dividing the SHWPs into more segments, thereby symmetrizing the radiation incident on the fiber-coupling optics, hence raising the fiber-coupling efficiency.

ACKNOWLEDGMENTS

The research was supported by the TKP2021 grant of NKFIH Hungary as a part of Project No. BME-NVA-02, and by the Quantum Informatics National Laboratory project, NKFIH-873-4/2020. The PHC phase compensator crystals were prepared using the infrastructure of ELI-ALPS Research Institute. The authors are extremely grateful to the colleagues of the mechanical and optical workshops of the Department of Atomic Physics, Dénes Varga, György Zemplényi, and Imre Tóth, who fabricated the custom parts of the equipment.

[1] A. K. Ekert, Quantum cryptography based on Bell's theorem, Phys. Rev. Lett. **67**, 661 (1991).

[2] R. Ursin, F. Tiefenbacher, T. Schmitt-Manderbach, H. Weier, T. Scheidl, M. Lindenthal, B. Blauensteiner, T. Jennewein, J. Perdigues, P. Trojek *et al.*, Entanglement-based quantum communication over 144 km, Nat. Phys. **3**, 481 (2007).

[3] J. Pseiner, L. Achatz, L. Bulla, M. Bohmann, and R. Ursin, Experimental wavelength-multiplexed entanglement-based quantum cryptography, Quantum Sci. Technol. **6**, 035013 (2021).

[4] J. L. O'Brien, Optical quantum computing, Science **318**, 1567 (2007).

[5] N. Takanashi, A. Inoue, T. Kashiwazaki, T. Kazama, K. Enbutsu, R. Kasahara, T. Umeki, and A. Furusawa, All-optical phase-sensitive detection for ultra-fast quantum computation, Opt. Express **28**, 34916 (2020).

[6] D. Bouwmeester, J.-W. Pan, K. Mattle, M. Eibl, H. Weinfurter, and A. Zeilinger, Experimental quantum teleportation, Nature (London) **390**, 575 (1997).

[7] Z.-D. Li, R. Zhang, X.-F. Yin, L.-Z. Liu, Y. Hu, Y.-Q. Fang, Y.-Y. Fei, X. Jiang, J. Zhang, L. Li *et al.*, Experimental quantum repeater without quantum memory, Nat. Photonics **13**, 644 (2019).

[8] P. G. Kwiat, K. Mattle, H. Weinfurter, A. Zeilinger, A. V. Sergienko, and Y. Shih, New High-Intensity Source of Polarization-Entangled Photon Pairs, Phys. Rev. Lett. **75**, 4337 (1995).

[9] P. G. Kwiat, E. Waks, A. G. White, I. Appelbaum, and P. H. Eberhard, Ultrabright source of polarization-entangled photons, Phys. Rev. A **60**, R773 (1999).

[10] F. Steinlechner, P. Trojek, M. Jofre, H. Weier, D. Perez, T. Jennewein, R. Ursin, J. Rarity, M. W. Mitchell, J. P. Torres *et al.*, A high-brightness source of polarization-entangled photons optimized for applications in free space, Opt. Express **20**, 9640 (2012).

[11] A. Villar, A. Lohrmann, and A. Ling, Experimental entangled photon pair generation using crystals with parallel optical axes, Opt. Express **26**, 12396 (2018).

[12] T. Kim, M. Fiorentino, and F. N. C. Wong, Phase-stable source of polarization-entangled photons using a polarization Sagnac interferometer, Phys. Rev. A **73**, 012316 (2006).

[13] F. Steinlechner, M. Gilaberte, M. Jofre, T. Scheidl, J. P. Torres, V. Pruneri, and R. Ursin, Efficient heralding of polarization-entangled photons from type-0 and type-II spontaneous parametric downconversion in periodically poled $KTiOPO_4$, J. Opt. Soc. Am. B **31**, 2068 (2014).

[14] H. Kim, O. Kwon, and H. S. Moon, Pulsed Sagnac source of polarization-entangled photon pairs in telecommunication band, Sci. Rep. **9**, 5031 (2019).

[15] A. Lohrmann, C. Perumangatt, A. Villar, and A. Ling, Broadband pumped polarization entangled photon-pair source in a linear beam displacement interferometer, Appl. Phys. Lett. **116**, 021101 (2020).

[16] C. Perumangatt, A. Lohrmann, and A. Ling, Experimental conversion of position correlation into polarization entanglement, Phys. Rev. A **102**, 012404 (2020).

[17] E. Knill, R. Laflamme, and G. J. Milburn, A scheme for efficient quantum computation with linear optics, Nature (London) **409**, 46 (2001).

[18] J. Chen, K. F. Lee, C. Liang, and P. Kumar, Fiber-based telecom-band degenerate-frequency source of entangled photon pairs, Opt. Lett. **31**, 2798 (2006).

[19] F. Basso Basset, M. B. Rota, C. Schimpf, D. Tedeschi, K. D. Zeuner, S. F. Covre da Silva, M. Reindl, V. Zwiller, K. D. Jöns, A. Rastelli, and R. Trotta, Entanglement Swapping with Photons Generated on Demand by a Quantum Dot, Phys. Rev. Lett. **123**, 160501 (2019).

[20] C. T. Holló, T. Sarkadi, M. Galambos, D. Bíró, A. Barócsi, P. Koppa, and G. Erdei, Compact, single-mode fiber-coupled, correlated photon pair source based on type-I beta-barium borate crystal, Opt. Eng. **61**, 025101 (2022).

[21] C. T. Holló, T. Sarkadi, M. Galambos, B. Bodrog, A. Barócsi, P. Koppa, and G. Erdei, Compact, portable, fiber-coupled correlated photon pair source with enhanced performance, in

Quantum 2.0 Conference and Exhibition (Optica Publishing Group, Washington, DC, 2022), p. QTu2A.18.

[22] Zemax opticstudio, https://www.zemax.com/products/opticstudio, accessed 06.05.2021.

[23] J. Altepeter, E. Jeffrey, and P. Kwiat, *Photonic State Tomography* (Academic Press, Cambridge, MA, 2005), pp. 105–159.

[24] C. Wagenknecht, C.-M. Li, A. Reingruber, X.-H. Bao, A. Goebel, Y.-A. Chen, Q. Zhang, K. Chen, and J.-W. Pan, Experimental demonstration of a heralded entanglement source, Nat. Photonics **4**, 549 (2010).

[25] C. Erven, C. Couteau, R. Laflamme, and G. Weihs, Entangled quantum key distribution over two free-space optical links, Opt. Express **16**, 16840 (2008).

[26] J. Lee, L. Shen, A. Cerè, J. Troupe, A. Lamas-Linares, and C. Kurtsiefer, Symmetrical clock synchronization with time-correlated photon pairs, Appl. Phys. Lett. **114**, 101102 (2019).